23rd ABCM International Congress of Mechanical Engineering
December 6-11, 2015, Rio de Janeiro, RJ, Brazil

SIMULATION STUDY OF BIOMASS POWDER COMBUSTION IN A CYCLONIC FURNACE

Rodrigo Cavalcanti Ribeiro Lima
Rene Francisco Boschi Gonçalves
Faculdade de Engenharia Mecânica – Universidade Federal do Pará – R. Augusto Corrêa, 1 - Guamá, Belém - PA, CEP 66075-110.
rodcribeiro@gmail.com
renefbg@gmail.com

Manoel F. M. Nogueira
Faculdade de Engenharia Mecânica – Universidade Federal do Pará – R. Augusto Corrêa, 1 - Guamá, Belém - PA, CEP 66075-110.
mfmn@ufpa.br

Danielle R. S. Guerra
Faculdade de Engenharia Mecânica – Universidade Federal do Pará – R. Augusto Corrêa, 1 - Guamá, Belém - PA, CEP 66075-110.
daguerra@ufpa.br

Abstract. *The thermal energy in the form of heat generally is produced and provided through thermal plants by combustion using coal, a type of fuel which impacts the environment severely. An effective way for reducing the specific consumption of coal is the preheating of the air intake system, which is responsible for increasing the flame temperature, a fundamental parameter in the control reactions that occur internally. The current study presents the computational modeling of a horizontal cyclonic furnace burning biomass powder, using for this the ANSYS FLUENT software. The mathematical models selected for the simulation were described as well as the boundary conditions. The obtained results are presented through velocity profiles and vectors, temperature fields and charts of species mass fractions. The temperature fields showed a maximum close to 1800 K, while charts with mass fraction of species have demonstrated that, with the combustible and initial conditions set, the combustion reaction occurs completely at 0.4 m, which contrasts with the analyzed reactor length of 2 m. The velocity field presents a peak of 63.74 m/s and velocity vectors revealed the presence of recirculating of the gas combustion reaction products. This feature is directly related to the NOx formation, increasing the residence time of the product combustion gases at higher temperatures. The main mechanism of NOx formation was identified as the thermal mechanism.*

Keywords: *biomass combustion simulation, cyclonic furnace modelling, reactant flow, Euler-Lagrange model.*

1. INTRODUCTION

Modeling and simulation can be helpful for optimizing the biomass cyclonic furnace design and its operation with minimal temporal and financial costs. However, it is a complex work due to the multiphase reactive turbulent flows involving different physical-chemistry interactions. Because of the need to deal with a non-conventional type, the horizontal cyclonic furnace analyzed in this study does not present information in the literature. Furthermore, the high temperatures impede the measurement of operating parameters inside the reactor. Thus, this study intends to provide information of the furnace combustion process and auxiliary in its experiments and design.

The combustion in a cyclonic furnace promotes the burning of solid particles in suspension. It is a cylindrical chamber where the fuel particulate is tangentially injected with the air resulting in the burning in cyclonic motion. Because of the high relative speed of gas-particles provided by this type of injection, high heat and mass transfer coefficients are caused. The difference in density between the particles of biomass and the air causes the particles to be thrown to the wall of the combustor while the air is pushed to the center, causing the combustion to occur in the boundary layer near the wall.

Multiphase flows can be classified based on the description of the solid phase in two approaches: Eulerian–Eulerian (EEM), a continuum approach for both phases (Zhou, 2015); Eulerian–Lagrangian (ELM), a continuum approach for the fluid and a discrete particle method for solid phase (Adamczyk, *et al.*, 2014; Ma, *et al.*, 2009; Bonefacic, *et al.*, 2015). The EEM approach averages both fluids and solids by a statistical procedure and treats the solids phase as a pseudo continuum (Xie, *et al.*, 2012). According to Zhou (2015), "the key problem of this modeling is the closure models of particle turbulence (particle turbulent fluctuation), leading to particle diffusion/dispersion".

In the ELM approach, the fluid phase is treated as a continuum and calculated in the Eulerian frame of reference, while the motion and combustion of the solid fuel particles are tracked in the Lagrangian reference frame. There is

constant exchange of momentum, mass, and heat between the combusting gas and solid particles and the exchanges between the two systems appear as source/sink terms in the governing equations for the continuous gas phase flows as well as those for the discrete solid particles (Adamczyk, *et al.*, 2014; Ma, *et al.*, 2009).

De Souza, *et al*., 2010, performed a simulation of a vertical cyclonic furnace with adiabatic walls burning biomass particles, and compared results obtained from cases with different models of turbulence (k-ε RNG and Reynolds Stress Model), and radiation (P-1 and DO). Júnior (2011) analyzed the characteristics of the reactive flow of methane and air, and reported on the influence of air staged supply in cyclonic furnace focused in NO_x production. Kops and Malte (2004) reports combustion simulations of wood dust and the generation of NO_x in cyclone burners, showing the detailed chemical model of thermal mechanism of NOx formation and fuel mechanism, comparing results for different fuels and turbulence models.

This paper presents the development of an ELM computational modelling of the horizontal cyclonic furnace, aiming to understand the main characteristics of the combustion processes, velocity and temperature distributions as well as the pollutant NO_x formation. Thus, it will allow for the acquisition of preliminary results of the process with low financial costs and time. Additionally, it will aid in the realization of experimental tests with greater accuracy.

2. METHOD

In the cyclonic furnace, a premixed mixture of biomass powder and air are insulated by the feeding system through a single entry into the reactor. This initiates the combustion process influenced by diffusion of heat and species, which occurs in three steps: dry, devolatilization and combustion of the volatiles and char, yielding ash and some gases. Nevertheless, the reaction model utilized in the simulation was the species transport model.

The ELM approach was used to solve the multiphase reactive flow. The biomass particles were treated as a dispersed phase and their trajectories were computed in a Lagrangian frame by a balance force particle equation. A non-spherical drag law was used based on the correlation of Haider and Levenspiel (1989). The shape factor, $\emptyset$, assumed as 0.366, is the ratio between the surface area of a sphere having the same volume as the particle and the actual surface area of the particle. A heating balance is solved and the net heat of the particle appears as a source or sink of heat in subsequent calculations of the continuous phase energy equation. The devolatilization process is solved with the single kinetic rate devolatilization model, which assumes that the rate of devolatilization is first-order dependent on the amount of volatiles remaining in the particle (Fluent, 2011). The kinetic/diffusion-limited model solves the heterogeneous one-step surface reaction of the char.

The gas phase is treated as a continuum by solving conservation equations of mass, species, momentum, and energy. The turbulence-chemistry interaction of the gas phase was modeled by finite-rate/eddy-dissipation sub-model. In this method both the Arrhenius and eddy-dissipation reaction rates are calculated and the net reaction rate is taken as the minimum of these two rates, which is more realistic because it prevents that the reactants burn as soon as they enter the computational domain, upstream of the flame stabilizer. A two-step reaction is used to model the homogeneous reaction of the gas phase. The turbulence model used is the k-ε Re-Normalisation Group (RNG). Recent works (Kops and Malte, 2004; De Souza, *et al*., 2010) demonstrated that this turbulence model provides a good concordance to predict the cyclonic behavior in reactive flows. Due to the presence of solid particles in the flow, the effects of the thermal radiation was not neglected, and the P1 method was used to solve the gray radiation model based on De Souza, *et al.* (2010).

2.1 Gas phase

The conservation equations for chemical species Eq. (1) predicts the local mass fraction of each specie through the solution of a convection-diffusion equation for the *i*th species.

$$\frac{\partial(\rho_g Y_{g,i})}{\partial t} + \nabla.\left(\rho_g Y_{g,i} u_g\right) = -\nabla.\vec{J_i} + R_i + S_i \tag{1}$$

Where $Y_{g,i}$ is the mass fraction of each gas species. R_i is the net rate of production of species i by chemical reaction, calculated by the finite-rate/eddy-dissipation model. S_i is the rate of creation by addition from the dispersed phase. The term $\vec{J}_i$ is the diffusion flux of species i and is described by Eq. (2) to turbulent flows.

$$\vec{J_i} = -\left(\rho_g D_{i,m} + \frac{\mu_t}{S_{c_t}}\right)\nabla Y_{g,i} - D_{T,i}\frac{\nabla T}{T} \tag{2}$$

The term S_{Ct} is the turbulent Schmidt number, related with the turbulent viscosity, μ_t, and the turbulent diffusivity, D_t, through the correlation $\mu_t/\rho_g D_t = S_C$. The standard value 0.7 to the Schmidt number is assumed in this work.

In the finite-rate/eddy-dissipation model, the net reaction rate is taken as the minimum of the Arrhenius Eq. (3) and eddy-dissipation, Eq. (5) and Eq. (6), reaction rates. “In practice, the Arrhenius rate acts as a kinetic switch, preventing

reaction before the flame holder. Once the flame is ignited, the eddy-dissipation rate is generally smaller than the Arrhenius rate, and reactions are mixing-limited" (Fluent, 2011).

$$R_i = k_f \prod_{j=1}^{N} [C_j]^{(n'_j + n''_j)} \tag{3}$$

In Eq. (3), C_j is the molar concentration of species j, n'_j and n''_j are the rate exponents for reactant and product species, respectively. The rate constant k_f is computed using the Arrhenius expression by Eq. (4).

$$k_f = A T^{\beta} e^{-E/RT} \tag{4}$$

Where A is pre-exponential factor, β is the temperature exponent, E is the activation energy for the reaction and R is the universal gas constant. In the eddy-dissipation model the net rate of production of species i, R_i, is given by the smaller of the Eq.(5) and Eq. (6).

$$R_i = v'_i M_{w,i} A \rho \frac{\varepsilon}{k} \min_{\mathcal{R}} \left(\frac{Y_{\mathcal{R}}}{v'_{\mathcal{R}} M_{w,\mathcal{R}}} \right) \tag{5}$$

$$R_i = v'_i M_{w,i} A B \rho \frac{\varepsilon}{k} \frac{\sum_P Y_P}{\sum_j^N v''_j M_{w,j}} \tag{6}$$

Where Y_p is the mass fraction of any product species, Y_R is the mass fraction of a particular reactant, and A and B are empirical constants equal to 4.0 and 0.5, respectively.

2.2 Solid phase

In the Eulerian-Lagrangian approach the trajectory of the discrete phase particle is predicted by integrating the force balance on the particle, which is written in a Lagrangian reference frame. This force balance equates the particle inertia with the forces acting on the particle (Fluent, 2011). This balance is presented in Eq. (7) for the direction in Cartesian coordinates.

$$\frac{du_p}{dt} = F_D(\vec{u} - \vec{u}_p) + \frac{\vec{g}(\rho_p - \rho)}{\rho_p} \tag{7}$$

The term $F_D(\vec{u} - \vec{u}_p)$ represents the drag force per unit particle mass and

$$F_D = \frac{18\mu}{\rho_p d_p^2} \frac{C_D Re}{24} \tag{8}$$

Here, $\vec{u}$ is the fluid phase velocity, $\vec{u}_p$ is the particle velocity, μ is the molecular viscosity of the fluid, ρ is the fluid density, ρ_p is the density of the particle, and d_p is the diameter of a sphere having the same volume of the particle. *Re* is the relative Reynolds number, which is defined as

$$Re \equiv \frac{\rho d_p |\vec{u}_p - \vec{u}|}{\mu} \tag{9}$$

The drag coefficient, C_D, for the non-spherical particle is calculated with the correlation of Haider and Levenspiel (1989). In this approach, the shape factor, $\varnothing$, is the ratio between the surface area of a sphere having the same volume as the particle and the actual surface area of the particle. The value assumed for $\varnothing$ is 0.366.

2.2.1 Heating balance

The heat lost or gained by the particle as it traverses each computational cell appears as a source or sink of heat in subsequent calculations of the continuous phase energy equation.

$$m_p c_p \frac{dT_p}{dt} = h A_p (T_\infty - T_p) + \varepsilon_p A_p \sigma (\theta_R^4 - T_p^4) \tag{10}$$

Where m_p is the mass of the particle, c_p is the heat capacity, A_p is the surface area, T_∞ is the local temperature of the continuous phase, h is the convective heat transfer coefficient, ε is the particle emissivity, σ is the Stefan-Boltzmann constant.

The radiation temperature, θ_R, was calculted as $\theta_R = \left(\frac{G}{4\sigma}\right)^{1/4}$, where G is the incident radiation and was calculated as $G = \int_{\Omega=4\pi} Id\Omega$. I is the radiation intensity and Ω is the solid angle.

The heat transfer coefficient, h, is evaluated by Eq. (25).

$$Nu = \frac{hd_p}{k_\infty} = 2{,}0 + 0{,}6Re_d^{1/2}Pr^{1/3} \tag{11}$$

The term, d_p, is the diameter of a sphere having the same volume of the particle, k_∞ is the thermal conductivity of the continuous phase, Re_d is the Reynolds Number based on the particle diameter and the relative velocity. Pr is the Prandtl number of the continuous phase.

2.2.2 Devolatilization

Based on recent studies (Kops and Malte, 2004; De Souza et al, 2010), the first order reaction model, described in Eq. (12), was used to predict the volatilization behavior.

$$\frac{dm_p(t)}{dt} = -k_v\left[m_p(t) - m_{p0}(1 - f_{v0})\right] \tag{12}$$

Where $k_v = A\exp(-E/RT)$ is a kinetic rate constant, $m_p(t)$ is the mass of the particle as a function of time. The terms m_{p0} and f_{v0} are the mass of particle and the mass fraction of volatiles, respectively, initially present in the particle. Values of $33884\ s^{-1}$ and $6{,}9e{+}7\ J/kgmol$ are implemented for the pre-exponential factor, A, and the activation energy, E, from the Arrhenius rate equation, based on the Kops and Malte (2004) studies.

2.2.3 Surface combustion

In simulation, after the volatilization process occurs, the particle is reduced to char and a surface reaction begins, which consumes the combustible fraction of the particle. The surface reaction mechanism was assumed as the one-step, irreversible reaction, and the char combustion rate is limited by the diffusion of oxygen through the boundary layer surrounding the particle.

2.2.4 NO_x formation

The primary nitrogen oxide from combustion systems is NO, and, in some systems, appreciable NO_2 is produced, usually as a result of NO + ½ O_2 → NO_2 conversion in low-temperature mixing regions of non-premixed systems (Turns, 2012).

According to Junior (2011), typically the amounts of NO formed in the combustion are much higher than NO_2. However, once launched in the atmosphere, NO rapidly becomes NO_2, and therefore NO_x emission rates are always calculated considering only its two compounds as NO.

In the current simulation, only the thermal (Zeldovich) mechanism involving atmospheric nitrogen and a mechanism by which NO_x is formed by oxidation of nitrogen in the fuel are considered, and other paths by which NO_x can be produced, such as Fenimore (prompt) mechanism, N_2O-intermediate mechanism, and NNH mechanism, are disregarded.

2.3 Fuel Properts and equilibrium reaction analysis

The ultimate and proximate analysis of the fuel are obtained from the biomass characterization laboratory of the EBMA group in the UFPA. The mass fractions of the reactants and products of the equilibrium reaction combustion were calculated with the ComGas software, developed by Zarate, *et al.* (2008).

Table 1. Fuel Characteristics.

Ultimate	C	H	O	N	S
Analysis	0,4576	0,0647	0,4765	0,0010	0,0001
Proximate	Volatile	Fixed carbon	Ash	Moisture	HHV (kJ/kg)
Analysis	0,7210	0,1447	0,0085	0,1258	20100

Table 2. Equilibrium reaction mass fractions and temperatures.

Reactants				Reactants temperature (K)	Adiabatic flame temperature (K)
Fuel	H_2O	O_2	N_2		
0.0859	0.0124	0.2100	0.6917	300	1616.97

Products									
CO_2	CO	H_2O	H_2	OH	O_2	O	N_2	NO	SO_2
0.1441	7.43e-06	0.0620	1.8e-07	9.816e-05	0.1013	2.94e-06	0.6911	0.0015	1.717e-05

2.4 Computational domain, initial, and boundary conditions

The simulation was performed considering a steady state flow process. The inlet boundary conditions specify that a mass flow rate proportional to the area of the inlet surface enters the domain with a normal to boundary direction to the volatiles and air mixture, as well as to the discrete phase particles. The mass flow rate of the gas phase and discrete phase are set as 0.1711 kg/s and 0.015 kg/s, respectively. The wall is considered to be adiabatic. For the outlet boundary condition backflow parameters were adopted based on the product species from the equilibrium combustion reaction and the adiabatic flame temperature.

The mass flow rate at the inlet and the equivalence ratio were set according to the operational parameters used on the experimental procedure in the real cyclonic combustor, and a low equivalence ratio is adopted due to limitations in the supply system. A schematic drawing with dimensions and the computational mesh are shown in Fig. 1 and Fig. 2, respectively. The numerical grid was constructed as a non-structured mesh with 216,456 elements and 42,376 nodes.

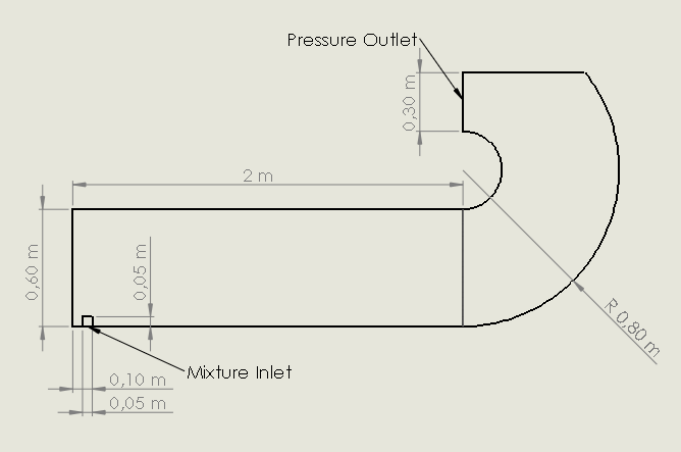

Figure 1. Image of the real cyclonic combustor.

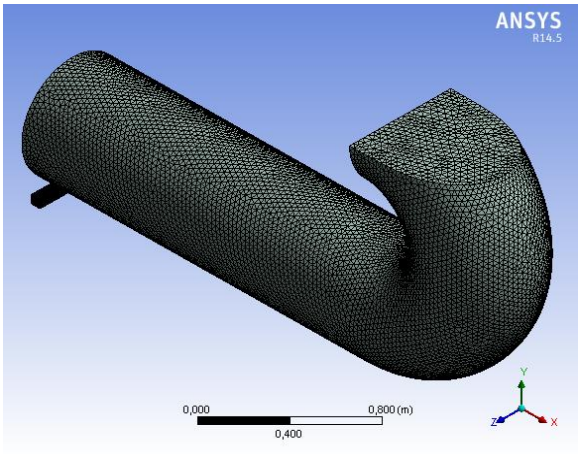

Figure 2. Computational mesh.

2.5 Numerical solution

The gas phase equations are discretized in finite volume form with staggered scalar and momentum nodes. A Coupled solution scheme is used to adjust pressure and gas velocity to satisfy gas continuity. The steady-state solution is computed using second-order discretization for all equations. The PRESTO algorithm was used to predict the pressure behavior. Courant number and some under-relaxation factors were adjusted to provide stable solutions.

3. RESULTS AND DISCUSSIONS

The simulation allowed for the prediction of the flow behavior in the cyclonic furnace, including the occurrence of backflow, which is characteristic of cyclonic flows. The results could not be validated by experimental data due to lack of equipment that would enable the measurements inside the reactor.

In the cyclonic furnace, the mixture of particles, volatiles, and air enters the combustion chamber flowing tangentially to the wall with a spiral trajectory along the burner length. The analysis of velocity and pressure profiles showed that the cyclonic flow of fluid tangentially to the wall produces the appearance of a radial pressure gradient inside the combustion chamber, causing the pressure in the center to be less than the pressure close to the wall chamber. The velocity vectors distribution in Fig. 3 shows that this behavior causes a backflow, which begins near to the outlet of reactor, from the wall toward the center, and interacts with the helical flow at the interface between the flows, creating vortices that improve the influence of turbulence in the heat transfer inside the reactor. The main contribution of this

reflux is the heating of reactants entering the reactor, causing the increase in average temperature of the combustion reaction.

Figure 3 shows a longitudinal plane with velocity vectors colored by velocity magnitude scale. The peak of velocity is *63.74 m/s* and occurs in the mixture inlet. The highest velocity magnitudes are in the boundary layer at the beginning of the reactor. The limits of pressure obtained in the simulation range from *-123.98 Pa* to *877.55 Pa*.

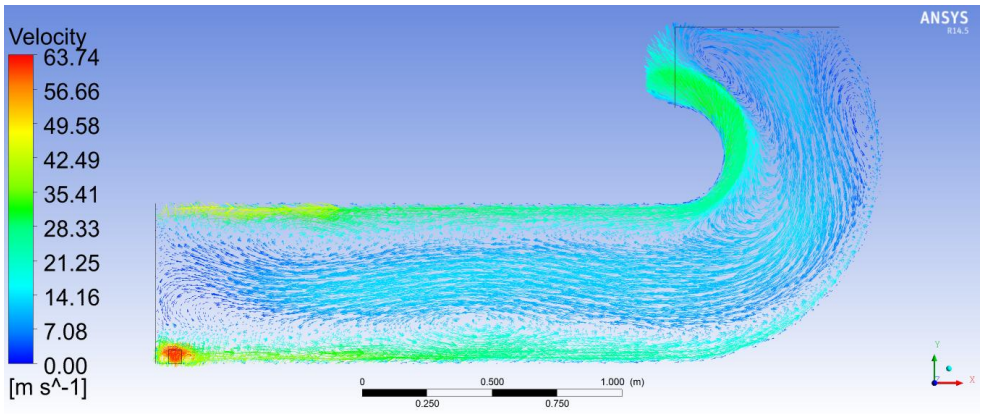

Figure 3. Velocity vectors in a longitudinal central plane.

Due to the difference in density of the phases, the biomass particles are thrown against the wall of the reactor, and the air is pushed to the center, causing the combustion reaction to occur in the region near the wall when it achieves a local stoichiometric equivalence ratio. Figure 4 shows that the region with highest temperature occurs near the wall.

The temperature limits calculated in the simulation range from *298 K* to *1797 K*. Figure 4 presents a longitudinal plane of temperature. A reduced range in color map, from *1200 K* to *1700 K*, was used to better observe the qualitative behavior of the temperature distribution.

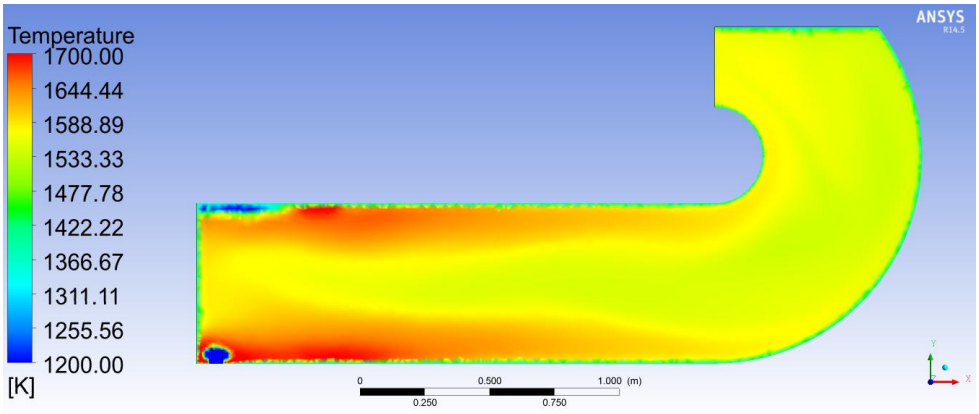

Figure 4 – Plane of temperature field.

The region with the lowest temperatures, below *1360 K*, at the top of the beginning of the reactor, shows a cross section of the flame front propagation. This zone is composed of a mixture of reactants and a small proportion of the products, which enter by diffusion inside the flame. Otherwise, the surface of the flame is composed of a mixture of reactants in stoichiometric equivalence ratio and flame temperature. A flame propagation is supported by heating transfer (conduction and radiation) and molecular diffusion, where both are flowing to the center of the flame, making the reagent mixture reach the necessary ignition energy and burn at the flame surface.

Figure 5 shows a temperature distribution plane in a transversal section at *0.08 m* of the beginning of the reactor. Through it, it is possible to observe the development of the combustion reaction and the flame front propagation. When entering the reactor, the mixture initiates the chemical reaction based on the results of the Finite Rate model because this provides a smaller chemical kinetics rate. This zone of lower temperature characterizes the ignition delay. Upon reaching the upstream flame, the reaction becomes driven by EDM, and thus becomes mixing limited.

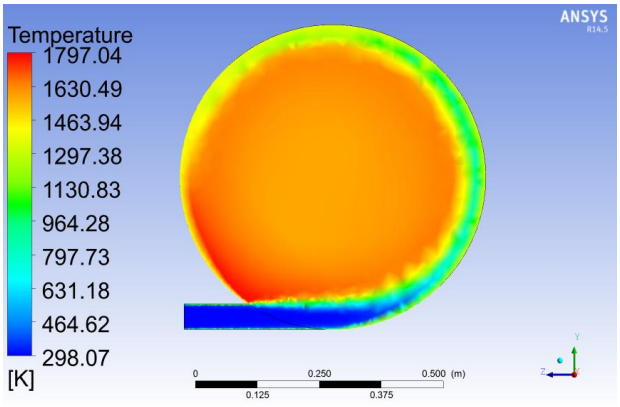

Figure 5. Plane of temperature in a cross section at 0.08 m.

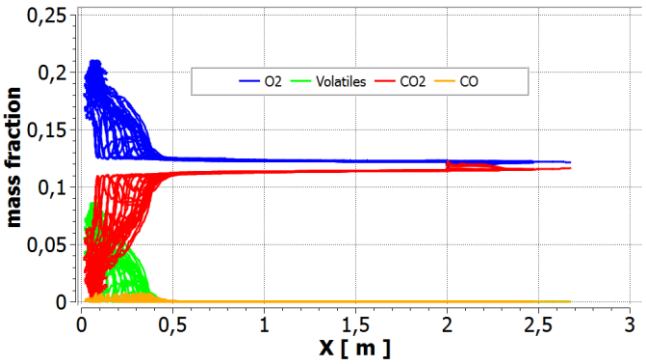

Figure 6. Mass fraction of species along the x axis reactor.

The flame is propagated to approximately 0.4 m length of the reactor, at which point the reacting species are extinguished, leaving only the minimum mass fraction of oxygen, due to lean-combustion reaction, and products, as shown in Fig. 6.

Figure 6 shows a chart with the mass fractions of volatile, oxygen, carbon monoxide, and carbon dioxide as a function of reactor length. The presence of maximum values of reactants (oxygen and volatile) and minimum product (carbon monoxide and carbon dioxide) is observed at the beginning of the reactor. While the combustion reaction develops, a decrease in mass fraction of reactants and an increase of the presence of products are detected. Next to *0.4 m* point, the mass fractions of the species assumes constant values, with the extinction of volatiles, signaling the end of the combustion reaction. Through this, it can be inferred that the reaction has entered in equilibrium, allowing a comparison with the results obtained with the ComGas, except NOx production, which should be considered the contribution of the thermal mechanism formation. The CO content in the gas concentration is relatively low and can be seen in the chart of fig. 5, and its extinction means that complete combustion has occurred, as a typical result of reactions with low equivalence ratio.

NO formation was predicted based on the thermal and fuel mechanisms. Figure 7 shows a longitudinal plan with velocity vectors colored by distribution of mass fraction of NO. Through that, it can be observed that the NO begins to form in the region of flame, which presents a mass fraction close to $1.5e^{-03}$, which is the value calculated by Comgás for equilibrium reactions.

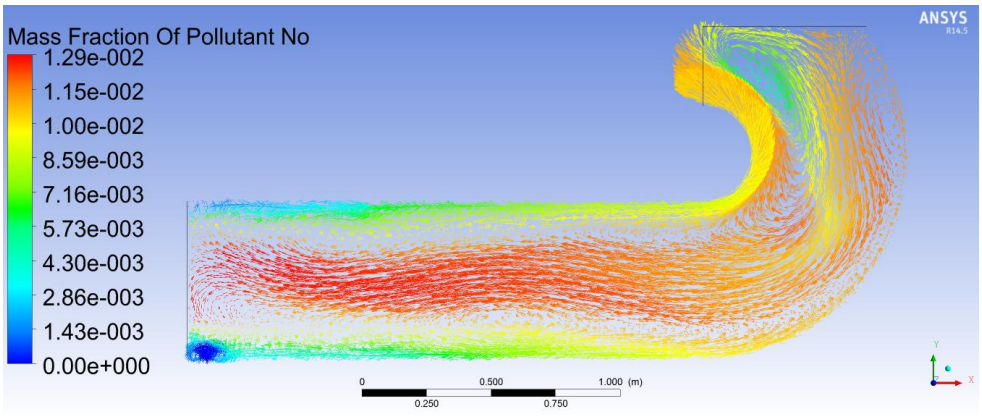

Figure 7. Velocity vectors colored by mass fraction of NO distribution.

As previously noted, the helical flow follows the reactor wall and reaches the pressure outlet region causing a reverse flow coming from the wall to the center of the reactor, returning to the mixture inlet zone. With the velocity vectors distribution of Fig. 7, it can be observed that the mass concentration of NO increases along this flow, proportionally to the residence time inside the reactor at high temperatures, characterizing the behavior of the thermal mechanism formation. The graphs of Fig. 8 and 9 shows the mass concentration of HCN, from the fuel mechanism of NO formation, with the length x-axis Cartesian coordinates. With it, it can be observed that the formation of HCN is concentrated near the flame region, where there is the existence of volatile, and is consumed shortly after this area.

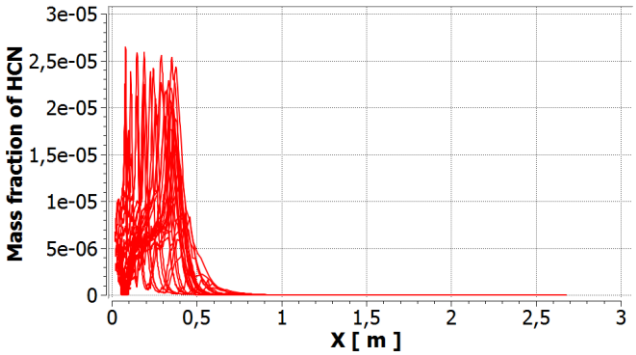

Figure 8. Chart of mass fraction of HCN.

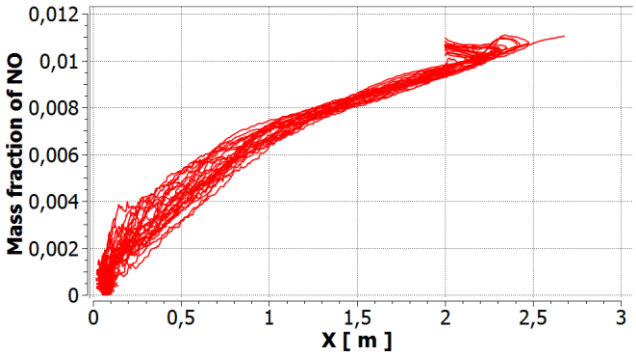

Figure 9. Chart of mass fraction of NO.

4. CONCLUSIONS

The cyclonic furnace behavior was predicted and the results of mass fractions of species demonstrated a good concordance with the results of equilibrium reaction. The NO mass fraction near the flame zone was close to the equilibrium reaction results and the formation of the NO via thermal mechanism was evaluated for the entire flow. Thus, the simulation permitted the observation that the backflow causes the improvement on the residence time of the nitrogen in the reactor, which results in the improvement of NO production. The simulation also allowed the association between the formation of NO and the reactor length. The charts of mass fraction of species and temperature profile enabled the prediction of the required length of the reactor where the combustion is totally complete, and in this case is approximately *0.4 m* from the beginning of the reactor.

5. REFERENCES

Adamczyk, W.P., Klimanek, A., Białecki, R.A., Wecel, G., Kozołub, P. and Czakiert, T., 2014. *Comparison of the standard Euler–Euler and hybrid Euler–Lagrange approaches for modeling particle transport in a pilot-scale circulating fluidized bed*. Particuology – Elsevier LTD, 2014.

Ansys Fluent Theory Guide, Release 14.0, Ansys Inc, November 2011.

Bonefacic, I., Frankovic, B. and Kazagic, A., 2015. *Cylindrical particle modelling in pulverized coal and biomass co-firing process.* Applied Thermal Engineering – Elsevier LTD, 2015.

De Souza, R.T., Marques L.C., Castelo, A.M., Guerra, D.R.S. and Nogueira, M.F.M., 2010. "Escoamentos bi-fásico, sólido-ar, em combustores ciclônicos". In *VII Escola de Primavera de Transição e Turbulência – EPTT 2010*. Ilha Solteira – SP, Brazil.

Haider, A. and Levenspiel, O., 1989. *Drag coefficient and terminal velocity of spherical and nonspherical particles*. Powder Technology, 1989.

Júnior, A.M.C.B., 2011. *Análise das características de escoamento e da influência do estagiamento do ar de combustão sobre a emissão de nox em uma caldeira ciclônica: simulação cfd da combustão de gás metano*. Graduate thesis, Universidade Federal do Pará, Belém.

Kops, S.M.B. and Malte, P.C., 2004. "Simulation and Modeling of Wood Dust Combustion in Cyclone Burners – Final Technical Report". U. S. Department of Energy, January, 2004.

Ma, L., Gharebaghi, M., Porter, R., Pourkashanian, M., Jones, J.M. and Williams, A., 2009. *Modelling methods for co-fired pulverized fuel furnaces*. Fuel – Elsevier LTD, 2009.

Turns, S.R., 2012. *An introduction to combustion: Concepts and applications.* Mc Graw Hill, New York, 3rd edition.

Xie, J., Zhong, W., Jin, B., Shao, Y. and Liu, H., 2012. *Simulation on gasification of forestry residues in fluidized beds by Eulerian–Lagrangian* approach. Bioresource Technology – Elsevier LTD, 2012.

Zarate, H. M. R., Itai Y., Nogueira, M. F. M., Moraes, S. B. and Rocha, B. R. P., 2008. "Predictions of the Products Compositions for Combustion or Gasification of Biomass and others Hydrocarbons". In *Proceedings of the 12th Brazilian Congress of Thermal Sciences and Engineering - ENCIT2008.* Belo Horizonte, Brazil. 2008

Zhou, L., 2015. "Two-phase turbulence models in eulerian-eulerian simulation of gas-particle flows and coal combustion". In *The 7th World Congress on Particle Technology - WCPT7*. Beijing, China.

6. RESPONSIBILITY NOTICE

The authors are the only responsible for the printed material included in this paper.